



**HAL**  
open science

# Stacking order-dependent sign-change of microwave phase due to eddy currents in nanometer-scale NiFe/Cu heterostructures

O. Gladii, R L Seeger, L. Frangou, G. Forestier, U. Ebels, S. Auffret, Vincent Baltz

► **To cite this version:**

O. Gladii, R L Seeger, L. Frangou, G. Forestier, U. Ebels, et al.. Stacking order-dependent sign-change of microwave phase due to eddy currents in nanometer-scale NiFe/Cu heterostructures. *Applied Physics Letters*, 2019, 115, pp.032403. 10.1063/1.5093150 . hal-02022873v3

**HAL Id: hal-02022873**

**<https://hal.science/hal-02022873v3>**

Submitted on 15 Jul 2020

**HAL** is a multi-disciplinary open access archive for the deposit and dissemination of scientific research documents, whether they are published or not. The documents may come from teaching and research institutions in France or abroad, or from public or private research centers.

L'archive ouverte pluridisciplinaire **HAL**, est destinée au dépôt et à la diffusion de documents scientifiques de niveau recherche, publiés ou non, émanant des établissements d'enseignement et de recherche français ou étrangers, des laboratoires publics ou privés.

# Stacking order-dependent sign-change of microwave phase due to eddy currents in nanometer-scale NiFe/Cu heterostructures

Cite as: Appl. Phys. Lett. **115**, 032403 (2019); doi: [10.1063/1.5093150](https://doi.org/10.1063/1.5093150)

Submitted: 18 February 2019 · Accepted: 25 June 2019 ·

Published Online: 18 July 2019



View Online



Export Citation



CrossMark

O. Gladii,<sup>a)</sup> R. L. Seeger,<sup>a)</sup> L. Frangou,<sup>a)</sup> G. Forestier, U. Ebels, S. Auffret, and V. Baltz<sup>b)</sup>

## AFFILIATIONS

Univ. Grenoble Alpes, CNRS, CEA, Grenoble INP, IRIG-SPINTEC, F-38000 Grenoble, France

<sup>a)</sup>Contributions: O. Gladii, R. L. Seeger, and L. Frangou contributed equally to this work.

<sup>b)</sup>[vincent.baltz@cea.fr](mailto:vincent.baltz@cea.fr)

## ABSTRACT

In the field of spintronics, ferromagnetic/nonmagnetic metallic multilayers are core building blocks for emerging technologies. Resonance experiments using stripline transducers are commonly used to characterize and engineer these stacks for applications. Up to now in these experiments, the influence of eddy currents on the excitation of the dynamics of ferromagnetic magnetization below the skin-depth limit was most often neglected. Here, using a coplanar stripline transducer, we experimentally investigated the broadband ferromagnetic resonance response of NiFe/Cu bilayers a few nanometers thick in the sub-skin-depth regime. Asymmetry in the absorption spectrum gradually built up as the excitation frequency and Cu-layer thickness increased. Most significantly, the sign of the asymmetry depended on the stacking order. Experimental data were consistent with a quantitative analysis considering the eddy currents generated in the Cu layers and the subsequent phase shift of the feedback magnetic field generated by the eddy currents. These results extend our understanding of the impact of eddy currents below the microwave magnetic skin-depth and explain the line shape asymmetry and phase lags reported in stripline experiments.

Published under license by AIP Publishing. <https://doi.org/10.1063/1.5093150>

Resonance experiments are a powerful means to study physical systems and facilitate advances in material characterization and engineering. In the field of spintronics, ferromagnetic/nonmagnetic (F/NM) metallic multilayers are core building blocks for emerging technologies.<sup>1</sup> In these multilayers, the physical properties of the F (effective magnetization, anisotropy, damping), the NM metal (spin penetration length, relaxation mechanisms, eddy currents), and the interface (spin filtering, roughness) can all be recorded by measuring the ferromagnetic resonance (FMR) spectra and determining their position (resonance field), linewidth, and line shape.<sup>2</sup>

Line shape asymmetries are relatively common in FMR experiments performed with stripline setups (coplanar and microstrip).<sup>3–7</sup> The part of the stripline inductively coupled to the sample is equivalent to a device circuit defining a complex microwave impedance.<sup>3,8,9</sup> The resulting phase of the microwave excitation leads to an absorption-dispersion admixture and produces asymmetric line shapes. Although a phenomenological parameter accounting for such asymmetry is considered to extract the resonance field and linewidth from data fitting, it is usually not commented on. The reason for this is because in most cases, the asymmetry, linewidth, and resonance field are not related, and because for most geometries the absorption

component prevails.<sup>3</sup> This type of “experiment-related asymmetry” is therefore small.

Other effects such as eddy currents may produce unusual line shapes. This type of effect has been thoroughly studied for film thicknesses above the skin-depth limit.<sup>10</sup> In contrast, below this limit, the effects of eddy currents were most often neglected, except for a study on ac charge currents, including currents produced by spin pumping and spin-charge conversion<sup>11</sup> and for a series of comprehensive studies focused on microwave screening/shielding,<sup>3,9,12,13</sup> e.g., leading to layer-transducer ordering-dependent standing spin wave modes in sufficiently thick layers<sup>3,12</sup> and to depth-dependent dephasing.<sup>13</sup> As we will further discuss below, eddy currents need to be carefully considered to accurately determine damping<sup>14,15</sup> and other related spintronic properties,<sup>16</sup> especially when characterizing low-damping materials. Some recent experimental studies on F-NiFe(10 nm)/NM-(Au,Cu) bilayers<sup>17,18</sup> revealed how the Oersted field—due to eddy currents in the NM layer—affects the dynamics of F magnetization, and more specifically, how it distorts the resonance line shape. The experiments were performed in a cavity setup and corroborated the results of analytical calculations. The scenario considered in Refs. 17 and 18 involved eddy currents in the NM conductor, generated by a

homogeneous excitation radio frequency magnetic field ( $\mathbf{h}_{rf}$ ) applied out-of-plane. The phase shift ( $\varphi$ ) between  $\mathbf{h}_{rf}$  and the eddy current-induced field out-of-plane ( $\mathbf{h}_{ind} = \mu\mathbf{h}_{rf}e^{i\varphi}$ ) resulted in an absorption( $A$ )-dispersion( $D$ ) admixture of the signal. It produced an asymmetric resonance line, related to the absorbed power,  $P \propto A + \beta D$  with

$$\beta = \frac{\mu \sin(\varphi)}{1 + \mu \cos(\varphi)} + \beta_0, \quad (1)$$

where  $\beta_0$  is the empirical residual “experiment-related” phase shift.  $P$  can be calculated from:  $P \propto \text{Re}[i\omega(\chi h_{rf})h_{rf}^*]$ , where the magnetic susceptibility  $\chi$  is deduced from the Landau-Lifshitz-Gilbert equation. In this scenario relying on the use of homogeneous  $\mathbf{h}_{rf}$  out-of-plane, experiments conducted with stripline setups, with  $\mathbf{h}_{rf}$  in the sample plane, should not generate eddy currents in the conductive layers. However, it has been suggested that sample tilting would lead to an out-of-plane component,<sup>7</sup> thus creating the conditions for “eddy current-related asymmetry.” According to this hypothesis, the sign of the asymmetry should be independent of the stacking order for the layers, because the homogeneous  $\mathbf{h}_{rf}$  generates eddy currents with  $\mathbf{h}_{ind}$  pointing in the same direction above and below the NM conductor. The data show that this assumption fails to completely describe the experimental results.

In this article, the incompletely understood impact of eddy currents is investigated and we unravel the contributions to the line shape asymmetry in stripline experiments. The full stacks used in this study were (from substrate to surface): Cu( $t_{Cu}$ )/NiFe( $t_{NiFe}$ )/Al(2)Ox and NiFe( $t_{NiFe}$ )/Cu( $t_{Cu}$ )/Al(2)Ox (nm) multilayers.  $t_{Cu}$  is the thickness of the Cu layer and was varied between 1 and 14 nm;  $t_{NiFe}$  is the thickness of the NiFe layer:  $t_{NiFe} = 4, 8, \text{ or } 12$  nm. Stacks were deposited at room temperature by dc-magnetron sputtering on Si/SiO<sub>2</sub>(500) substrates at a pressure of argon of  $2.3 \times 10^{-3}$  mbar. The NiFe layer was deposited from a Ni<sub>81</sub>Fe<sub>19</sub> (at. %) permalloy target. A 2-nm-thick Al cap was deposited to form a protective Al(2)Ox film after oxidation in air. This insulating film also prevented electrical contact between the samples and the waveguide [Figs. 1(a) and 1(b)]. Unless specified otherwise, the sample dimensions were:  $l = 4$  mm and  $w = 3$  mm. The microwave transducer consisted of a double-ground plane broadband coplanar waveguide. The width of the central conductor strip was  $375 \mu\text{m}$  and the gap between the lines was:  $g = 140 \mu\text{m}$ . A Schottky diode was used for detection. Modulation coils and lock-in detection were used to enhance the signal-to-noise ratio. FMR experiments and the corresponding differential absorption spectra,  $d\chi''/dH \propto dP/dH$  vs  $H$  [Figs. 1(c)–1(h)], were recorded at room temperature at frequencies ranging between 4 and 20 GHz.

First, we discuss the spectrum asymmetry which gradually built up as the  $t_{Cu}$  increased [Figs. 1(c)–1(h)]. This behavior revealed a non-negligible impact of eddy currents circulating in the Cu layers. Most importantly, the sign of the asymmetry depended on the ordering of the Cu and NiFe layers, i.e., whether the Cu layer was the buffer or the capping layer. Figure 2(a) illustrates a mechanism where the inhomogeneous field of the coplanar waveguide, with the out-of-plane components, generates eddy currents with oppositely directed induced in-plane fields ( $\mathbf{h}_{ind}$ ) above and below a Cu layer. By further considering a phase shift between  $\mathbf{h}_{rf}$  and  $\mathbf{h}_{ind}$ , one can write:  $\mathbf{h}_{ind}^{\pm} = \mu\mathbf{h}_{rf}e^{i\varphi^{\pm}}$ . The superscripts “+” and “−” relate to the “capping” and “buffer” cases, respectively. We get a situation similar to Ref. 17, described by

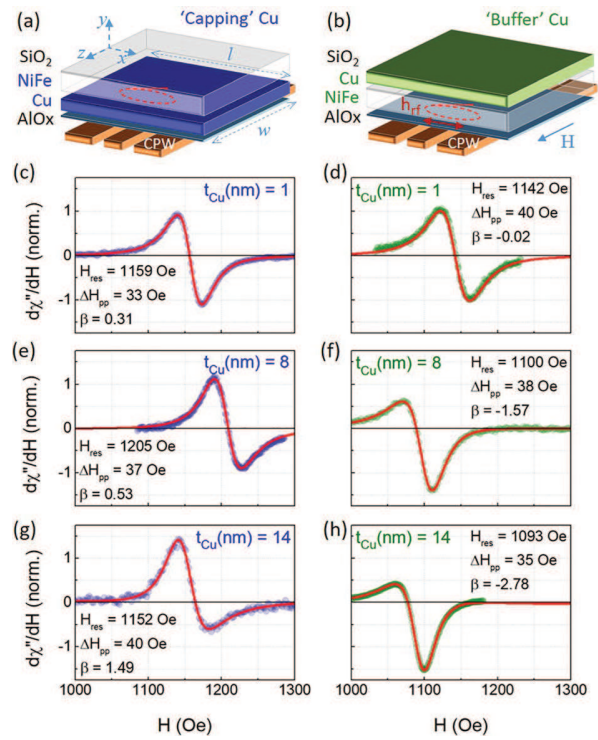


**FIG. 1.** (a) and (b) Schematic representations of the coplanar waveguide (CPW)—FMR experiment. Samples were placed face-down on the waveguide. The in-plane dc bias field ( $H$ ) and the in-plane component of the excitation magnetic field from the waveguide ( $\mathbf{h}_{rf}$ ) are represented. (c)–(h) Representative differential absorption spectra ( $d\chi''/dH$  vs  $H$ ) measured for Si/SiO<sub>2</sub>/NiFe(8)/Cu( $t_{Cu}$ )/Al(2)Ox and Si/SiO<sub>2</sub>/Cu( $t_{Cu}$ )/NiFe(8)/Al(2)Ox (nm) stacks. The solid lines were fitted to the data using a model derived from Ref. 17, which is described in the text. Data-fitting allowed the resonance field ( $H_{res}$ ), the peak-to-peak linewidth ( $\Delta H_{pp}$ ), and the asymmetry parameter ( $\beta$ ) to be determined.

Eq. (1), but considering that the dominant coupling occurs between the FMR mode and the in-plane fields. To extract the asymmetry and quantify the findings, the differential resonance spectra were fitted using the following equation:<sup>17</sup>  $\frac{d\chi''}{dH} \propto \frac{d}{dH} \left[ \frac{1 + \beta(H - H_{res}) / (\sqrt{3}\Delta H_{pp})}{(H - H_{res})^2 + (\sqrt{3}\Delta H_{pp}/2)^2} \right]$ , where  $H_{res}$  is the resonance field, and  $\Delta H_{pp}$  is the peak-to-peak linewidth.

Figure 2(b) shows  $\beta$  plotted as a function of  $t_{Cu}$  for a series of Cu( $t_{Cu}$ )/NiFe( $t_{NiFe} = 4, 8, 12$ )/Al(2)Ox (buffer) and NiFe( $t_{NiFe} = 4, 8, 12$ )/Cu( $t_{Cu}$ )/Al(2)Ox (nm) (capping) multilayers. The gradual increase in  $|\beta|$  with  $t_{Cu}$  agrees with the fact that eddy currents relate to the conductance of the Cu layers, which increases with  $t_{Cu}$ . The above deductions can be correlated by using Eq. (1). The field  $\mathbf{h}_{ind}$  relates to the rate of change of magnetic flux through the area,  $S$ , delimited by the eddy current loop. It can be expressed as  $\mathbf{h}_{ind} = \mu_0 2\pi f \frac{t_{Cu}}{P} a(l, w, g) \mathbf{h}_{rf}$ . We considered that the eddy current was given by  $I = S 2\pi f \mathbf{h}_{rf} / R$ , where the numerator corresponds to the electromotive force due to variations of  $\mathbf{h}_{rf}$  over time. The resistance of the loop of length  $P$ , is given by  $R = \rho P / (t_{Cu} \zeta)$ , where  $\zeta$  is the width of the loop, the spatial profile of which depends on the sample’s geometry in a nontrivial manner.<sup>19</sup> The averaged magnetic field acting on the NiFe layer is expressed as  $\mathbf{h}_{ind} = \mu_0 I / b$ , where  $b$  is a function of the geometry of the sample.

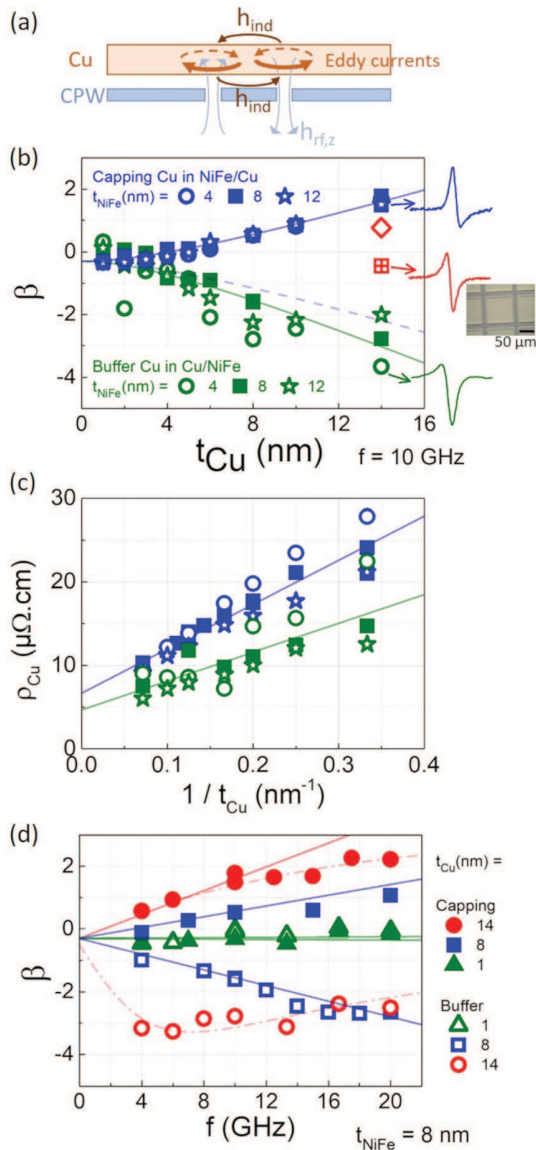


**FIG. 2.** (a) Illustration of a mechanism where the inhomogeneous field ( $\mathbf{h}_{rf}$ ) of the coplanar waveguide, with strong out-of-plane components, generates eddy currents with oppositely directed induced in-plane fields ( $\mathbf{h}_{ind}$ ) above and below a Cu layer. (b) Representative series of dependences of  $\beta$  on capping and buffer Cu-layer thickness ( $t_{Cu}$ ) for  $\text{Si}/\text{SiO}_2/\text{Cu}(t_{Cu})/\text{NiFe}(t_{\text{NiFe}} = 4; 8; 12)/\text{Al}(2)\text{Ox}$  and  $\text{Si}/\text{SiO}_2/\text{NiFe}(t_{\text{NiFe}} = 4; 8; 12)/\text{Cu}(t_{Cu})/\text{Al}(2)\text{Ox}$  (nm) stacks. Data were recorded at 10 GHz. The square crossed symbol corresponds to data recorded after patterning (inset) the  $\text{Cu}(14)/\text{Al}(2)\text{Ox}$  bilayer in a  $\text{Si}/\text{SiO}_2/\text{NiFe}(8)/\text{Cu}(14)/\text{Al}(2)\text{Ox}$  (nm) stack. The open square symbol corresponds to data for the same stack on which the whole etching process was performed. As these samples were protected by a resist they remained unpatterned. (c) Corresponding dependences of Cu-layer resistivity ( $\rho_{Cu}$ ) on  $t_{Cu}$ , obtained separately using standard 4-point electrical measurements. The lines were obtained using linear fits. (d) Representative series of dependences of  $\beta$  on frequency ( $f$ ) for  $\text{Si}/\text{SiO}_2/\text{Cu}(t_{Cu} = 1; 8; 14)/\text{NiFe}(8)/\text{Al}(2)\text{Ox}$  and  $\text{Si}/\text{SiO}_2/\text{NiFe}(8)/\text{Cu}(t_{Cu} = 1; 8; 14)/\text{Al}(2)\text{Ox}$  (nm) stacks. The solid lines in (b) and (c) were obtained using the model described in the text. The dashed and dash-dotted lines are visual guides.

The geometry-dependence of the parameters, including  $S\zeta/(bP) \equiv a(l, w, g)$  (dimension of length) will be discussed further below. Over the thickness range investigated (1–14 nm), the Cu layer's resistivity is given by  $\rho_{Cu}^{\pm} = \rho_0^{\pm} + \eta^{\pm}/t_{Cu}$ , where  $\eta^{\pm} = 3\lambda_{mfp}^{\pm}/8$  according to the Fuchs-Sondheimer model.<sup>20,21</sup> From separate 4-point electrical measurements, we obtained  $\rho_{Cu}^{+} [\mu\Omega\cdot\text{cm}] = 7 + 53/t_{Cu} [\text{nm}]$  for the capping layers and  $\rho_{Cu}^{-} [\mu\Omega\cdot\text{cm}] = 5 + 35/t_{Cu} [\text{nm}]$  for the buffer layers [Fig. 2(c)], which produce reasonable values for the electron mean free path:  $\lambda_{mfp}^{+} = 14$  nm and  $\lambda_{mfp}^{-} = 9$  nm. With regard to the phase shift ( $\varphi$ ) in Eq. (1), we neglected the contribution of the skin effect, which is proportional to  $t_{Cu}/\delta_{Cu}$ ,<sup>22</sup> because  $t_{Cu} = 1$ –14 nm, and the skin-depth  $\delta_{Cu} \sim 1000$ –500 nm for  $f = 4$ –20 GHz. In the ideal situation of a negligible inductive contribution to the complex impedance,  $\varphi^{+} = \pi/2$  for the capping layer case (quadrature phase shift because  $\mathbf{h}_{ind}$  is related to the time derivative of  $\mathbf{h}_{rf}$ ), and  $\varphi^{-} = -\pi/2$  for the buffer layer case (antiphase to the capping layer case). Developing the different terms in Eq. (1) produced a predictable nonlinear dependence of  $\beta$  on  $t_{Cu}$ , and a linear dependence on  $f$ ,

$$\beta^{\pm} = \pm\mu_0 2\pi f \frac{t_{Cu}}{\rho_0^{\pm} + \eta^{\pm}/t_{Cu}} a(l, w, g) + \beta_0. \quad (2)$$

The two solid lines in Fig. 2(b) were fitted with Eq. (2);  $a(l, w, g)$  and  $\beta_0$  were the only free parameters. It can be seen that the simplified model captures the physics of the phenomenon observed experimentally. Data fitting returned  $\beta_0 = -0.3$  and  $a(l, w, g) = 185 \pm 3 \mu\text{m}$  in both cases, in agreement with the constant sample dimensions in these sets of experiments. Remarkably, the model can account for the difference in the thickness-dependence of Cu-resistivity due to the inversion of the growth order. To emphasize this, the dashed line in Fig. 2(b) corresponds to a simulation using Eq. (2), considering the fictitious case of  $\rho_{Cu}^{+} = \rho_{Cu}^{-}$ . From Fig. 2(b), we note that slight deviations between predictions and experimental data can still be observed for the buffer layer case. Most importantly for thick Cu layers—as for example experimentally shown in Ref. 17 in the 10–50 nm range—and high frequencies, inductive contributions to the complex impedance are very likely to affect the ideal thickness-dependence of  $\beta$  in a nontrivial manner. Considering such a term, the phase shift becomes:  $\varphi = \pm\pi/2 + \theta(f, t_{Cu}, l, w, g)$ , where  $\theta$  shows a nonlinear dependence on several parameters, thus producing nonlinear dependences of  $\beta$  [from Eq. (1)].

The nontrivial influence of the inductive contributions to the complex impedance can clearly be seen for  $f$ -dependent measurements. Figure 2(d) shows  $\beta$  vs  $f$ , for a series of  $\text{Cu}(t_{Cu} = 1; 8; 14)/\text{NiFe}(8)/\text{Al}(2)\text{Ox}$  buffer and  $\text{NiFe}(8)/\text{Cu}(t_{Cu} = 1; 8; 14)/\text{Al}(2)\text{Ox}$  (nm) capping multilayers. Data for  $t_{Cu} = 1$  nm, in the absence of eddy current, correspond to  $\beta_0$  and superimpose for the buffer and capping cases. The  $f$ -dependence of  $\beta_0$  is weak, ruling out any  $f$ -dependent impedance contribution of the NiFe layer to the phase shift. The solid lines in Fig. 2(d) were produced by calculations using Eq. (2). The same set of parameters as that returned from Fig. 2(b) was used. It concurrently described the thickness- and  $f$ -dependences of  $\beta$  for the capping case [Fig. 2(d)], confirming that the simplified model reflects the physics behind the phenomenon observed. The overall linear increase in  $|\beta|$  with  $f$ , driven by the fact that eddy currents increase when the rate of change of flux rises, may be altered by complex inductive contributions, which are known to increase for higher frequencies and thicker films. In agreement with this information, we observe in



Fig. 2(d) that data depart from a linear dependence above 10 GHz for the 14-nm-thick layers, a result that contrasts with those obtained for the 8-nm-thick ones, which follow a linear dependence throughout. The 14-nm-thick buffer layer case typically illustrates how nontrivial contributions can drastically distort and bend the initially linear  $f$ -dependence. To rule out any contribution of the Si/SiO<sub>2</sub>(500) substrate on the sign-change of  $\beta$ , we compared a Cu(14)/NiFe(4)/Al(2)Ox to a NiFe(4)/Cu(14)/Al(2)Ox (nm) stack deposited on glass substrates (not shown). The same trend of a positive vs negative value of  $\beta$  for the capping vs buffer case was obtained.

We will now consider finite-size effects. Once again using Fig. 2(b), we will briefly comment on the square crossed symbol corresponding to data recorded after patterning only the Cu(14)/Al(2)Ox capping layers in a Si/SiO<sub>2</sub>/NiFe(8)/Cu(14)/Al(2)Ox (nm) stack [inset of Fig. 2(a)]. A  $4 \times 3 \text{ mm}^2$  array of square dots with a lateral size of  $100 \mu\text{m}$  was fabricated. Following patterning, two effects compete with one another. First, the number of eddy current loops increases, and simultaneously, the path of each loop is constrained. The fact that patterning reduced  $\beta$  to a value close to  $\beta_0$  [Fig. 2(b)] shows that eddy currents cannot develop in the dots. This result indicates that the dot size was smaller than the width of the eddy current loop. We further assessed the dependence of  $\beta$  on the sample's geometry in Fig. 3(a). We considered geometry-dependent parameters,  $S\zeta/(bP) \equiv a(l, w, g)$  to account for the fact that the spatial profile of the eddy currents depends on the sample's geometry in a nontrivial manner. In particular, the width ( $\zeta$ ) and the circulation (determining  $S$  and  $P$ ) are unknown. In addition, the amplitude of  $I$  is likely inhomogeneous along the width  $\zeta$ , making it difficult to obtain an analytical expression

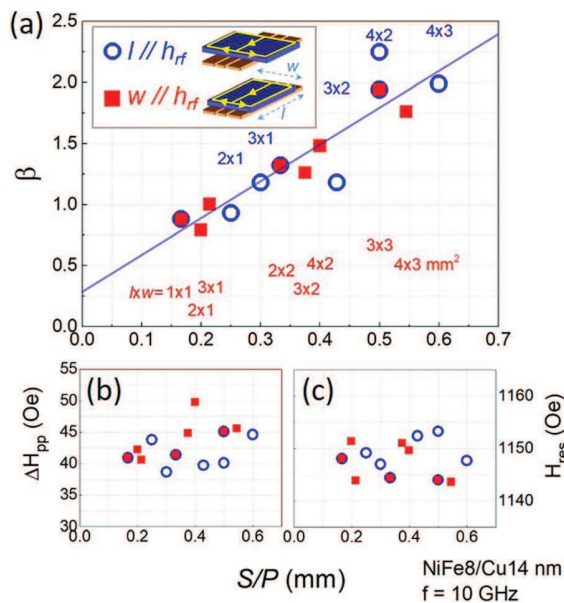


**FIG. 3.** (a) Dependences of  $\beta$  on the ratio  $S/P$  for Si/SiO<sub>2</sub>/NiFe(8)/Cu(14)/Al(2)Ox (nm) stacks for two sample's orientations:  $l // h_{rf}$  and  $w // h_{rf}$ .  $S$  is the area delimited by the eddy current loop and  $P$  is the length of the current path, considering that currents extend over the sample (see the inset). For  $l // h_{rf}$   $S/P = (w/2)/[2(w + l/2)]$ , and for  $w // h_{rf}$   $S/P = (lw/2)/[2(l + w/2)]$ . Data were recorded at 10 GHz. The line in (a) is a visual guide. (b,c) Corresponding dependences of  $H_{res}$  and  $\Delta H_{pp}$ .

for the parameter  $b$  relating to the magnetic field created by  $I$ . Considering the limit case when eddy currents extend over the full sample [inset in Fig. 3(a)], we obtained a linear dependence on  $S/P$  [Fig. 3(a)], meaning that  $\zeta/b$  seems to be almost independent of the geometry. The discrepancy for the  $\beta_0$  intercept is probably related to a geometry-dependence close to the smallest dimensions that is likely to result in curve-binding. The results also show that rotating the sample in the plane of the stripline had no impact on the data [Fig. 3(a)], demonstrating that both the length and the width of the current path contribute to  $h_{ind}$ . The most relevant insight is that stacking order-, thickness-, and  $f$ -dependent measurements (Fig. 2) returned to the same value of  $a(l, w, g)$ , in agreement with the constant sample dimensions in these sets of experiments. The value of  $a \sim 185 \mu\text{m}$  is also in agreement with the order of magnitude that can be estimated from Ref. 17. Figures 3(b) and 3(c) present the control data showing that the sample vs stripline dimensions remained within a range where the linewidth ( $\Delta H_{pp}$ ) and resonance field ( $H_{res}$ ) were unaffected by geometrical effects.

Before concluding the paper, we will briefly comment on  $H_{res}$  and  $\Delta H_{pp}$ . The total Gilbert damping,  $\alpha$ , was calculated from the slope of  $f$ -dependent measurements ( $\Delta H_{pp}$  vs  $f$ ), from  $\Delta H_{pp} = \Delta H_{pp0} + 4\pi\alpha f / (\sqrt{3}|\gamma|)$ ,<sup>23</sup> where  $\Delta H_{pp0}$  is the inhomogeneous broadening<sup>24</sup> due to spatial variations in the magnetic properties (values of a few Oe were measured in our experiments) and  $\gamma$  is the gyromagnetic ratio (derived from the fit of the curve representing  $H_{res}$  vs  $f$ ). Plots representing  $H_{res}$  vs  $t_{Cu}$  and  $\alpha$  vs  $t_{Cu}$  are shown in Figs. 4(a), 4(b) and Figs. 4(c), 4(d), respectively. The data showed no obvious link between eddy currents in the Cu layers (spectrum asymmetry in Fig. 2), and the spectrum position,  $H_{res}$ . Regarding  $\alpha$ , eddy currents in conductors adjacent to a resonator, including the waveguide, were shown to contribute to a damping process due to losses via inductive coupling.<sup>14,15,25</sup> This phenomenon is referred to as radiation damping and can be expressed as  $\alpha^{rad} = \mu_0^2 \kappa \gamma M_S t_F w / (2Z_0 l)$ ,<sup>14</sup> where  $M_S$  is the saturation magnetization,  $t_F$  is the ferromagnet's thickness,  $Z_0$  is the impedance of the NM conductor, and  $\kappa$  accounts for the mode profile. For YIG(200)/Al<sub>2</sub>O<sub>3</sub>(30)/Pt(5–20) (nm) samples with  $M_S \sim 121 \text{ emu.cm}^{-3}$  and dimensions of  $2 \times 5 \text{ mm}^2$ , in-plane stripline FMR measurements showed that  $\alpha^{rad}$  due to eddy currents in the Pt capping layer can be up to  $3 \times 10^{-4}$ —for the 20 nm thick  $35\text{-}\Omega$  Pt layer.<sup>15</sup> From this value, considering the dependence of  $\alpha^{rad}$  on  $M_S$ ,  $t_F$ ,  $Z_0$  and the sample dimensions, and extrapolating to our case, we estimate a maximum value of  $\alpha^{rad}$  of  $1 \times 10^{-4}$  for the NiFe(12)/Cu(14) (nm) with  $M_S \sim 700 \text{ emu.cm}^{-3}$ , dimensions of  $3 \times 4 \text{ mm}^2$  and a resistance of the Cu layer of  $10 \Omega$ . This value of  $\alpha^{rad}$  is too small to influence the damping of our NiFe layers ( $\alpha \sim 6\text{--}8 \times 10^{-3}$ ). In fact, no obvious contribution of eddy currents to  $\alpha$  can be inferred from our data. However, given the orders of magnitude indicated above, radiation contribution due to eddy currents in NM layers will need to be carefully considered when extracting  $\alpha$  in several other cases. For example, with a fivefold increase in the NiFe layer thickness,  $\alpha^{rad}$  will become sizeable. In addition, an  $\alpha^{rad}$  of the order of few  $10^{-4}$  is already significant for materials exhibiting low intrinsic damping, such as the YIG insulator ( $\alpha \sim 6 \times 10^{-3}$ ),<sup>15</sup> the Co<sub>1.9</sub>Mn<sub>1.1</sub>Si half metal Heusler alloy ( $7 \times 10^{-4}$ ),<sup>26</sup> and the Co<sub>25</sub>Fe<sub>75</sub> bcc alloy ( $5 \times 10^{-4}$ ).<sup>27</sup> We finally note from Fig. 4 that, for  $t_{NiFe} = 4 \text{ nm}$ , a nonmonotonous dependence of  $H_{res}$  was observed. This behavior supports nonmonotonous dependence of the effective NiFe magnetization,  $M_{eff}$  [Figs. 4(e) and 4(f)]

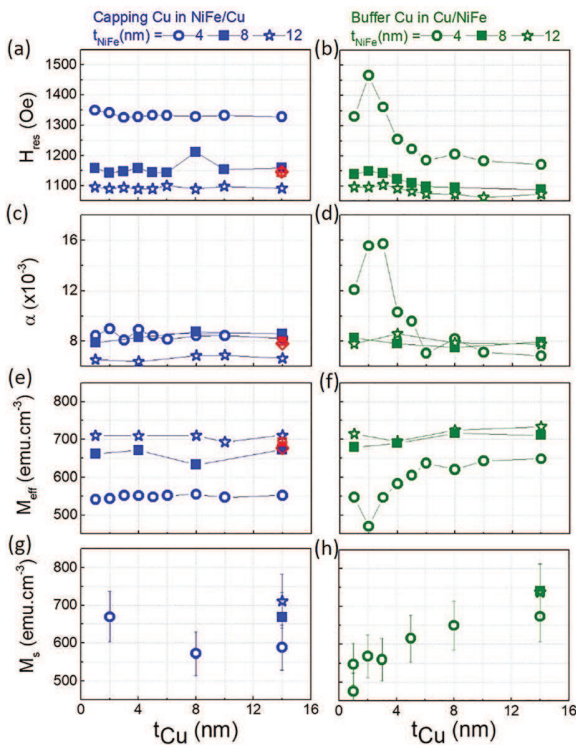


**FIG. 4.** Dependences of (a) and (b)  $H_{res}$ , (c) and (d)  $\alpha$ , (e) and (f)  $M_{eff}$ , and (g) and (h)  $M_S$  on  $t_{Cu}$  for  $\text{Si/SiO}_2/\text{Cu}(t_{Cu})/\text{NiFe}(t_{NiFe})/\text{Al}(2)\text{Ox}$  and  $\text{Si/SiO}_2/\text{NiFe}(t_{NiFe})/\text{Cu}(t_{Cu})/\text{Al}(2)\text{Ox}$  (nm) stacks. The square crossed symbols correspond to the patterned sample. (a)–(b) correspond to data recorded at 10 GHz. (c)–(d) were deduced from  $f$ -dependences of  $\Delta H_{pp}$ . (e) and (f) were deduced from  $f$ -dependences of  $H_{res}$ . (g) and (h) were measured independently by magnetometry, using a superconducting quantum interference device.

which can be extracted from  $H_{res}$  vs  $f$  using the Kittel formula<sup>28</sup>  $(2\pi f)^2 = |\gamma|H_{res}(H_{res} + 4\pi M_{eff})$ . We recall that  $M_{eff} = M_S - 2K_S/(4\pi M_S t_{NiFe})$ . The values of  $M_S$  [Figs. 4(g) and 4(h)], measured independently by magnetometry, were monotonous and thus confirmed that the nonmonotonous behavior of  $M_{eff}$  seems to primarily relate to the properties of the Cu/NiFe interface. A similar nonmonotonous dependence of  $\alpha$  was observed. Cu wets poorly on  $\text{SiO}_2$  compared to NiFe on  $\text{SiO}_2$  and Cu, and as a result may create rougher thin Cu films. Consequently, spatially inhomogeneous stray fields may lead to incoherent dephasing of the spin current<sup>29,30</sup> injected from the NiFe to the buffer Cu layer, and thus to enhanced damping.

In conclusion, the main contribution of this paper is that it represents systematic experimental evidence of a stacking-order-dependent sign-change of the microwave phase in nanometer-scale NiFe/Cu bilayers. The effect could be ascribed to eddy currents generated in the Cu layer in the sub-skin-depth regime by the time varying magnetic fields in the experiment. Distinct sets of experimental data were consistent with a simple quantitative analysis encompassing the main features of the phenomenon. These results contribute to our understanding of the impact of eddy currents below the microwave magnetic skin-depth and explain the contributions to the line shape asymmetry and phase lags reported in stripline experiments commonly used to characterize and engineer

materials for spintronic applications. They support a rational explanation to the use of the “phenomenological” parameter accounting for line shape asymmetry when extracting the spectral resonance field and linewidth from FMR data-fitting. The results also provide a straightforward way to detect the contributions of eddy currents from NM-adjacent conductors, as a caveat for the need in some cases to take these contributions into account when attempting to accurately determine damping<sup>14,15</sup> and other related spintronic properties such as spin-mixing conductance and the spin-Hall angle in spin-pumping experiments.<sup>16</sup>

We acknowledge financial support from the French national research agency (ANR) (Grant No. ANR-15-CE24-0015-01) and KAUST (Grant No. OSR-2015-CRG4-2626). We also thank M. Gallagher-Gambarelli for the critical reading of the manuscript.

## REFERENCES

- R. L. Stamps, S. Breitkreutz, J. Åkerman, A. V. Chumak, Y. Otani, G. E. W. Bauer, J. U. Thiele, M. Bowen, S. A. Majetich, M. Kläui *et al.*, *J. Phys. D: Appl. Phys.* **47**, 1 (2014).
- W. E. Bailey, *Introduction to Magnetic Random-Access Memory* (John Wiley & Sons, Ltd., 2016), p. 79.
- I. S. Maksymov and M. Kostylev, *Physica E* **69**, 253 (2015).
- A. Ghosh, S. Auffret, U. Ebels, and W. E. Bailey, *Phys. Rev. Lett.* **109**, 127202 (2012).
- A. Ghosh, J. F. Sierra, S. Auffret, U. Ebels, and W. E. Bailey, *Appl. Phys. Lett.* **98**, 052508 (2011).
- O. Mosendz, J. E. Pearson, F. Y. Fradin, G. E. W. Bauer, S. D. Bader, and A. Hoffmann, *Phys. Rev. Lett.* **104**, 046601 (2010).
- E. Montoya, T. Mckinnon, A. Zamani, E. Girt, and B. Heinrich, *J. Magn. Magn. Mater.* **356**, 12 (2014).
- W. Heinrich, *IEEE Trans. Microwave Theory Tech.* **41**, 45 (1993).
- M. Bailleul, *Appl. Phys. Lett.* **103**, 192405 (2013).
- F. J. Dyson, *Phys. Rev.* **98**, 349 (1955).
- A. J. Berger, E. R. J. Edwards, H. T. Nembach, A. D. Karenowska, M. Weiler, and T. J. Silva, *Phys. Rev. B* **97**, 94407 (2018).
- K. J. Kennewell, M. Kostylev, N. Ross, R. Magaraggia, R. L. Stamps, M. Ali, A. A. Stashkevich, D. Greig, and B. J. Hickey, *J. Appl. Phys.* **108**, 73917 (2010).
- W. E. Bailey, C. Cheng, R. Knut, O. Karis, S. Auffret, S. Zohar, D. Keavney, P. Warrnicke, J.-S. Lee, and D. A. Arena, *Nat. Commun.* **4**, 2025 (2013).
- M. A. W. Schoen, J. M. Shaw, H. T. Nembach, M. Weiler, and T. J. Silva, *Phys. Rev. B* **92**, 184417 (2015).
- M. M. Qaid, T. Richter, A. Müller, C. Hauser, C. Ballani, and G. Schmidt, *Phys. Rev. B* **96**, 184405 (2017).
- V. Vlaminck, J. E. Pearson, S. D. Bader, and A. Hoffmann, *Phys. Rev. B* **88**, 064414 (2013).
- V. Flovik, F. Macia, A. D. Kent, and E. Wahlstrom, *J. Appl. Phys.* **117**, 143902 (2015).
- V. Flovik, B. H. Pettersen, and E. Wahlström, *J. Appl. Phys.* **119**, 163903 (2016).
- M. Krakowski, *Arch. Elektrotech.* **64**, 307 (1982).
- K. Fuchs, *Math. Proc. Cambridge Philos. Soc.* **34**, 100 (1938).
- E. H. Sondheimer, *Adv. Phys.* **1**, 1 (1952).
- J. D. Jackson, *Classical Electrodynamics* (John Wiley & Sons, Ltd., 1962).
- C. E. Patton, *J. Appl. Phys.* **39**, 3060 (1968).
- E. Schlömann, *Phys. Rev.* **182**, 632 (1969).
- R. W. Sanders, D. Paquette, V. Jaccarino, and S. M. Rezende, *Phys. Rev. B* **10**, 132 (1974).
- S. Andrieu, A. Neggache, T. Hauet, T. Devolder, A. Hallal, M. Chshiev, A. M. Bataille, P. Le Fèvre, and F. Bertran, *Phys. Rev. B* **93**, 094417 (2016).
- M. A. W. Schoen, D. Thonig, M. L. Schneider, T. J. Silva, H. T. Nembach, O. Eriksson, O. Karis, and J. M. Shaw, *Nat. Phys.* **12**, 839 (2016).
- C. Kittel, *Phys. Rev.* **73**, 155 (1948).
- S. P. Dash, S. Sharma, J. C. Le Breton, J. Peiro, H. Jaffrès, J.-M. George, A. Lemaître, and R. Jansen, *Phys. Rev. B* **84**, 54410 (2011).
- Y. Tserkovnyak, A. Brataas, G. E. W. Bauer, and B. I. Halperin, *Rev. Mod. Phys.* **77**, 1375 (2005).